Available online at www.sciencedirect.com
SCIENCE DIRECT®
International Journal of Mass Spectrometry 235 (2004) 15–23
International Journal of Mass Spectrometry
www.elsevier.com/locate/ijms

Isomerization and dissociation of the acetonitrile molecular cation

Joong Chul Choe*

Department of Chemistry, University of Suwon, Suwon 440-600, South Korea

Received 26 February 2004; accepted 18 March 2004

Available online 4 May 2004

Abstract

The unimolecular dissociation of the acetonitrile molecular cation ($CH_3CN^{\bullet+}$) has been investigated using mass-analyzed ion kinetic energy spectrometry. Kinetic energy release distribution was obtained for the H loss. Density functional theory calculations have been performed to investigate isomerization and dissociation of $CH_3CN^{\bullet+}$. The potential energy surface (PES) for the H loss has been constructed from the calculations at the UB3LYP/6-311++G(3df,3pd) level. The RRKM model calculations based on the obtained PES predict that $CH_3CN^{\bullet+}$ interconverts to $CH_2CNH^{\bullet+}$ and $CH_2NCH^{\bullet+}$ followed by dissociation to a cyclic $C_2H_2N^+$ via a cyclic $C_2H_3N^{\bullet+}$ intermediate near the threshold. The present and previous experimental data for the dissociations of $C_2H_3N^{\bullet+}$ isomers are interpreted with the theoretical results.

Keywords: Acetonitrile ion; Isomerization; Unimolecular dissociation; DFT calculation

1. Introduction

Studies on acetonitrile molecular cation ($CH_3CN^{\bullet+}$, **1**) and its isomers have been extensively carried out using several mass spectrometric techniques including electron ionization (EI) [1–3], collision-induced dissociation (CID) [4–6], neutralization–reionization (NR) [6], metastable ion decomposition (MID) [4–6], photoionization (PI) [7], surface-induced dissociation (SID) [8], and atmospheric pressure photoionization [9]. Some stable isomers of $C_2H_3N^{\bullet+}$ have been suggested in the CID studies by two research groups [4,5], which include these four isomers:

$$\underset{\mathbf{1}}{[CH_3C{\equiv}N]^{\bullet+}} \quad \underset{\mathbf{2}}{[CH_2{=}C{=}NH]^{\bullet+}} \quad \underset{\mathbf{3}}{[CH_2{=}N{=}CH]^{\bullet+}} \quad \underset{\mathbf{4}}{[CH_3N{\equiv}C]^{\bullet+}}$$

Chess et al. [5] suggested that these four isomers are stable and interconversions of **1** and **2**, **1** and **4**, and **3** and **4** do not occur prior to dissociation. They pointed out an important fact that the CID spectra of $C_2H_2N^+$ generated by MID from the four isomers are identical and proposed a single cyclic structure for the $C_2H_2N^+$ ion. This implies that the four stable $C_2H_3N^{\bullet+}$ ions may isomerize to a common intermediate before the H loss, probably a cyclic structure at least in MID. Holmes and Mayer [6] suggested that **1** and **4** produce a single cyclic $C_2H_2N^+$ ion from the CID and NR spectra of source-generated $C_2H_2N^+$ ions. Contrary to the conclusion by Chess et al., Rider et al. [7] suggested that H atom migration in **1** occurs rapidly prior to dissociation from the PI data analysis for the productions of CH_3^+ and $CH_2^{\bullet+}$. In a recent SID work, Mair et al. [8] suggested that substantial numbers of **2** are formed from isomerization of **1** in the EI process.

Theoretical investigations on the dissociations of **1** have been limited comparing to the plentiful experimental ones. Only the results of quantum chemical calculations were reported for some $C_2H_3N^{\bullet+}$ [10] and $C_2H_2N^+$ [11–13] isomers. It is obvious that H atom migrations or CCN skeletal rearrangements are involved in the possible isomerizations of **1** to **2**, **3**, and **4**. Even though theoretical studies on H migration pathways of molecular cations containing oxygen atom such as acetaldehyde [14] and acetone [15] have been carried out, those of molecular cations containing nitrogen have been rare. It is worthwhile to investigate theoretically the pathways of isomerization and dissociation of **1**, which have not been understood clearly in the previous experimental studies. In this work, density functional theory (DFT) calculations are performed to predict the potential energy surface (PES) for isomerization and dissociation of the acetonitrile cation. The unimolecular dissociation, or MID, for the H loss is investigated using mass-analyzed ion kinetic

* Tel.: +82-31-220-2150; fax: +82-31-222-9385.
E-mail address: jcchoe@suwon.ac.kr (J.C. Choe).

1387-3806/$ – see front matter © 2004 Elsevier B.V. All rights reserved.
doi:10.1016/j.ijms.2004.03.003

energy spectrometry (MIKES) [16]. The present and previous experimental data will be interpreted with the kinetic modeling calculations based on the obtained PES.

2. Experimental

A double focusing mass spectrometer with reversed geometry (VG Analytical ZAB-E) was used for investigation. Acetonitrile or butyronitrile was introduced into the ion source via a septum inlet and ionized by 70 eV EI. The ion source temperature was maintained at 140 °C, and ions generated were accelerated to 8 keV. MIKES was used to observe the MIDs of the molecular ions. Namely, a precursor ion was selected by the magnetic sector and the translational kinetic energy of a product ion generated in the second field-free region of the instrument was analyzed by the electric sector. To improve the quality of a MIKE spectrum, signal averaging was carried out for repetitive scans. The MIKE profile of $C_2H_2N^+$ was recorded with an energy resolution higher than 4000 measured at half-height. The MIKE bandwidth at half-height of the precursor ion was 1.9 eV. Under this condition, deconvolution of the instrumental broadening was not needed in the calculation of kinetic energy release distribution (KERD) from the MIKE profile because the main beam bandwidth was negligible compared to that of $C_2H_2N^+$. Acetonitile and butyronitrile were of the best grade commercially available and used without further purification.

3. Computational

3.1. Quantum chemical calculation

Molecular orbital calculations were performed using the Gaussian 03 suite of programs [17]. Geometry optimizations for the several isomeric $C_2H_3N^{\bullet+}$ ions and fragments were carried out at the UB3LYP density functional levels of theory using the 6-311++G(3df,3pd) basis set. Transition state (TS) geometries connecting these structures were searched. The TS geometries found were checked by calculating the intrinsic reaction coordinates. The harmonic vibrational frequencies and the zero-point energies for the optimized structures were calculated at the UB3LYP/6-311++G(3df,3pd) level. These have not been scaled because the appropriate scaling factor at this level is not known though that of 0.9614 was recommended for the B3LYP/6-31G(d) level [18].

3.2. RRKM calculation of rate constants

The following RRKM expression was used to calculate the rate-energy dependences for various reactions involved [19,20].

$$k(E) = \sigma \frac{W^{\neq}(E - E_0)}{h\rho(E)} \quad (1)$$

Here, E and E_0 are the precursor ion internal energy and the critical energy for the reaction, respectively. $W^{\neq}$ is the sum of states at TS, ρ is the density of states of the reactant, and σ is the reaction path degeneracy. We could not locate transition states in quantum chemical calculations for the dissociation steps by H losses from **1**, **4**, and a cyclic $C_2H_3N^{\bullet+}$(**5**). It is usual in such a loose TS case to adjust the TS vibrational frequencies using the 1000 K activation entropy ($\Delta S^{\ddagger}$) [21,22]. Most of the $\Delta S^{\ddagger}$ values reported in Ref. [22] and in the subsequent works for the reactions occurring via a loose TS are in the range of 13–46 J mol^{-1} K^{-1} (3.0–11.0 eu). Therefore, a $\Delta S^{\ddagger}$ of 29 J mol^{-1} K^{-1} (7.0 eu) was used in the present RRKM rate calculations for the H losses. The results calculated using the limiting values of $\Delta S^{\ddagger}$ will be presented if needed.

3.3. Statistical calculation of KERD

The phase space theory (PST) was used to calculate the KERD expected for the statistical occurrence of the H loss from **1** via **5** [23–26].

$$n(T; J, E) \propto \int_{R_m}^{E-E_0-T} \rho_v(E - E_0 - T - R)\, P(T, J, R)\, dR \quad (2)$$

Here, T is the kinetic energy release (KER), and $n(T; J, E)$ is its distribution at the angular momentum J and the internal energy E of the precursor ion. The root-mean-square average J evaluated at the ion source temperature was used. ρ_v and P are the product vibrational and angular momentum state densities, respectively. R is the product rotational energy and R_m is its minimum.

4. Results and discussion

In the MID of **1** only the H loss was observed, agreeing with the previous experimental results [4,5]. The MID-MIKE spectrum is shown in Fig. 1(a) together with the profile of the precursor ion. To observe MID in conventional tandem mass spectrometry, the rate constant should be in the range 10^4 to 10^6 s^{-1}. In this work, the rate constant for the MID was estimated by varying the ion source acceleration voltage as suggested by Baer and coworkers [27,28]. It is $(1.2 \pm 0.4) \times 10^5$ s^{-1}. The available energy ($E - E_0$) for the H loss estimated from the MID-KERD is about 0.3 eV, which will be described below. The rate constant for the direct H loss from **1** was calculated using the RRKM formalism in Eq. (1). The vibrational frequencies used in the calculation are listed in Table 1. Even though the theoretical geometry of **1** deviates slightly from C_{3V} molecular symmetry as will be shown below, the reaction path degeneracy of **3** was used in the rate calculation for the reaction **1** → **a** + H$^{\bullet}$, which is more realistic. Since this reaction is a simple bond cleavage occurring via a loose

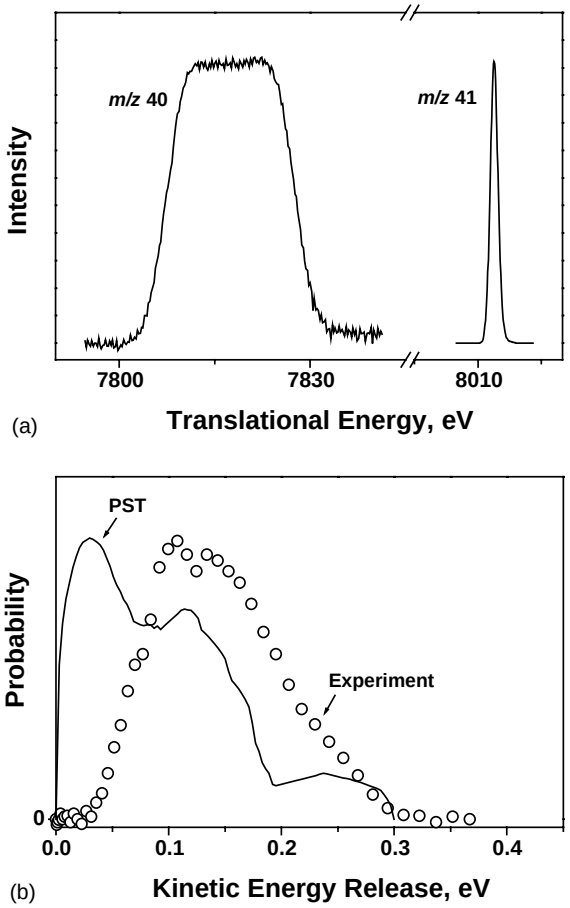

Fig. 1. (a) The MID-MIKE profile for the H loss from $CH_3CN^{\bullet+}$ generated by EI of acetonitrile. The profile of the precursor ion is also shown. The intensities of the two profiles are scaled to the same height. (b) The KERDs for the MID of H loss from $CH_3CN^{\bullet+}$. The experimental result evaluated for the profile in (a) is shown as circles. The PST calculation result using available energy 0.3 eV is shown as a solid curve.

TS, the TS vibrational frequencies were adjusted for $\Delta S^{\ddagger}$ to be 29 J mol^{-1} K^{-1}. The rate constant calculated thus is 2.7×10^9 s^{-1} at the available energy of 0.3 eV. Those calculated with $\Delta S^{\ddagger}$ of 13 and 46 J mol^{-1} K^{-1} are 5.5×10^8 and 1.7×10^{10} s^{-1} at the same energy, respectively. Namely, the theoretical rate constant is in the range of 5.5×10^8 to 1.7×10^{10} s^{-1}, much larger than the experimental one for the MID. Without consideration of the isomerization of **1** to a more stable ion(s) prior to dissociation the observed rate can not be explained. It is possible to produce other $C_2H_2N^+$ ions after the isomerization. First of all, the calculation results for possible isomerizations and dissociation pathways of **1** will be described.

4.1. DFT calculations

It is known that there are three stable $C_2H_2N^+$ isomers such as CH_2CN^+, CH_2NC^+, and a cyclic isomer, 1*H*-azirin-1-yl cation [11–13]:

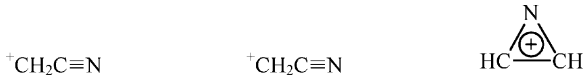

a **b** **c**

In the present quantum chemical calculations, the azirinyl cation, **c**, was found to be the most stable, agreeing with the recent result of high-level ab initio calculations by Mayer et al. [13] The optimized geometries of **a**–**c** are almost the same with those reported. The relative energies of the optimized species calculated in this work are listed in Table 2. Reliable experimental energy data for the species are very limited, which are included in the table. Energy at the zero point referred to that of **1**, and zero-point vibrational energies were added to calculate the relative energies.

Table 1
Molecular parameters used in the RRKM rate constant and PST KERD calculations

Species	
Vibrational frequency (cm^{-1})[a]	
1	184, 374, 447, 935, 1011, 1083, 1169, 1400, 2086, 2734, 2839, 3118
2	369, 394, 441, 557, 762, 1016, 1062, 1409, 2247, 3130, 3246, 3665
3	353, 411, 459, 753, 779, 1102, 1127, 1443, 2105, 3137, 3277, 3348
4	319, 319, 830, 1116, 1116, 1428, 1446, 1446, 2402, 3054, 3152, 3152
5	692, 739, 860, 878, 969, 1038, 1050, 1275, 1676, 3246, 3305, 3400
TS12	187, 325, 457, 919, 1012, 1013, 1411, 1900, 2537, 3100, 3226, 566*i*
TS47	207, 375, 711, 908, 1008, 1116, 1432, 1824, 2106, 3105, 3263, 1267*i*
TS56	685, 782, 869, 913, 1040, 1107, 1283, 1550, 2224, 3115, 3248, 1240*i*
c	867, 939, 992, 1008, 1177, 1385, 1683, 3207, 3258
Rotational frequency (cm^{-1})[a]	
1	5.18, 0.31, 0.31
c	1.31, 1.03, 0.57
Polarizability (10^{-24} cm^3)[b]	
H$^{\bullet}$	0.667

[a] DFT calculation at the UB3LYP/6-311++G(3df,3pd) level. *i* denotes imaginary frequency.
[b] Ref. [29].

Table 2
Relative energies and enthalpies of formation in kJ mol^{-1} of the relevant chemical structures

Species	Relative energy[a]	$\Delta_f H_{0K}$[b]
1 ($CH_3CN^{\bullet+}$)	0	1258(0)
2 ($CH_2CNH^{\bullet+}$)	−207	
3 ($CH_2NCH^{\bullet+}$)	−165	
4 ($CH_3NC^{\bullet+}$)	50	1262(4)
5 (c-$C_2H_3N^{\bullet+}$)	−32	
6	14	
7	92	
8	55	
TS12	82	
TS26	86	
TS28	83	
TS36	25	
TS37	131	
TS47	198	
TS56	139	
TS78	101	
a (CH_2CN^+) + $H^\bullet$	233	
b (CH_2NC^+) + $H^\bullet$	249	
c (c-$C_2H_2N^+$) + $H^\bullet$	191	
CH_3^+ + $CN^\bullet$	321	1535 (277)
$CH_2^{\bullet+}$ + HNC	350	1588 (330)
$CH_2^{\bullet+}$ + HCN	293	1522 (264)

[a] Theoretical result calculated at the UB3LYP/6-311++G(3df,3pd) density functional theory level. Energy at the zero point referred to that of **1**. Zero-point energies were added to calculate the relative energies. The calculated total energy and zero-point energy of **1** are −132.3646491 and 0.039592 hartrees, respectively.

[b] Enthalpy of formation at 0 K taken from Ref. [30]. The value in the parentheses denotes the enthalpy relative to **1**.

Figs. 2 and 3 show the lowest energy pathways of **1** and **4**, respectively, for formations of more stable isomers obtained from the DFT calculations. The optimized structure of **1** shows C_S molecular symmetry. One C–H bond (1.090 Å) is shorter than the other two C–H bonds (1.116 Å). The angle of CCN is 179.3°. The reduction of molecular symmetry from C_{3V} to C_S upon ionization of acetonitrile is probably due to the Jahn-Teller distortion suggested in the previous PI study [7]. **1** isomerizes to a ketenimine cation, **2** via **TS12** by two consecutive 1,2-H shifts. The critical energy (82 kJ mol^{-1}) for this isomerization is far smaller than that (233 kJ mol^{-1}) for the direct H loss to produce **a**. The calculated PES for the isomerizations of $C_2H_3N^{\bullet+}$ and some dissociation channels is depicted in Fig. 4. **2** is the most stable $C_2H_3N^{\bullet+}$ isomer found here. It forms an intermediate (**6**) having bended CNC structure by a 1,2-H shift and a subsequent rearrangement. **6** isomerizes further to two different stable cations. Very small energy barrier (11 kJ mol^{-1}) is needed to form a $CH_2NCH^{\bullet+}$ isomer (**3**) having linear CNC structure. On the other hand, the formation of a cyclic isomer, 1*H*-azirine cation (c-$C_2H_3N^{\bullet+}$, **5**) from **6**, which involves a H migration via a four-membered ring TS (**TS56**), needs cost of a considerable energy (125 kJ mol^{-1}). All the atoms of **5** are in the same plane except the H atom attached to the N atom. The calculated dihedral angle between the HNC and NCC planes is 120.2°. The cyclic $C_2H_2N^+$ ion, **c**, produced from **5** by the loss of H atom attached to the N atom, is more stable than **a** produced directly from **1** by 42 kJ mol^{-1} and than **b** from **4** by 58 kJ mol^{-1}.

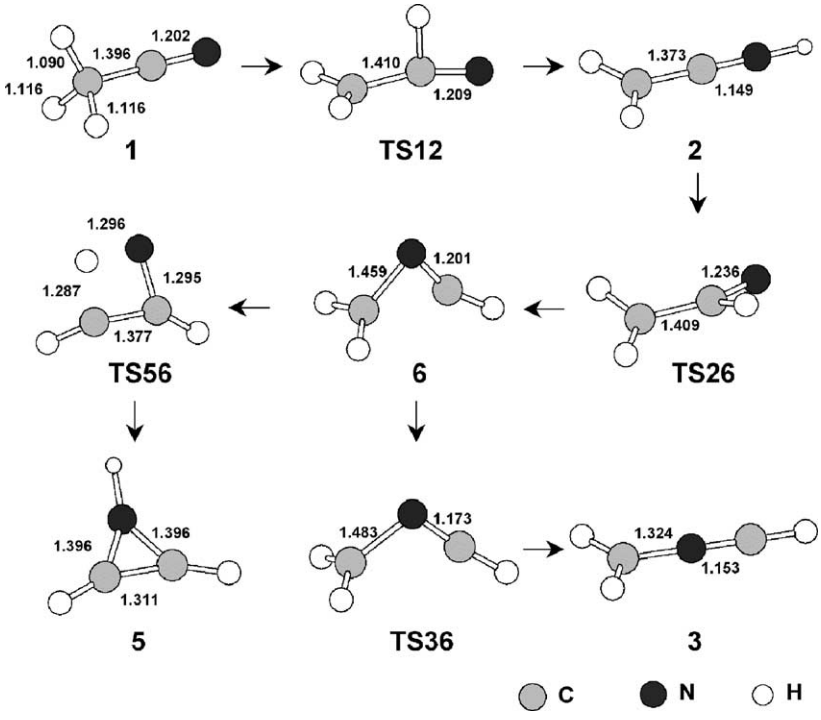

Fig. 2. The isomerization pathway of $CH_3CN^{\bullet+}$ obtained by DFT/UB3LYP/6-311++G(3df,3pd) calculations. The numbers are the bond lengths in Å.

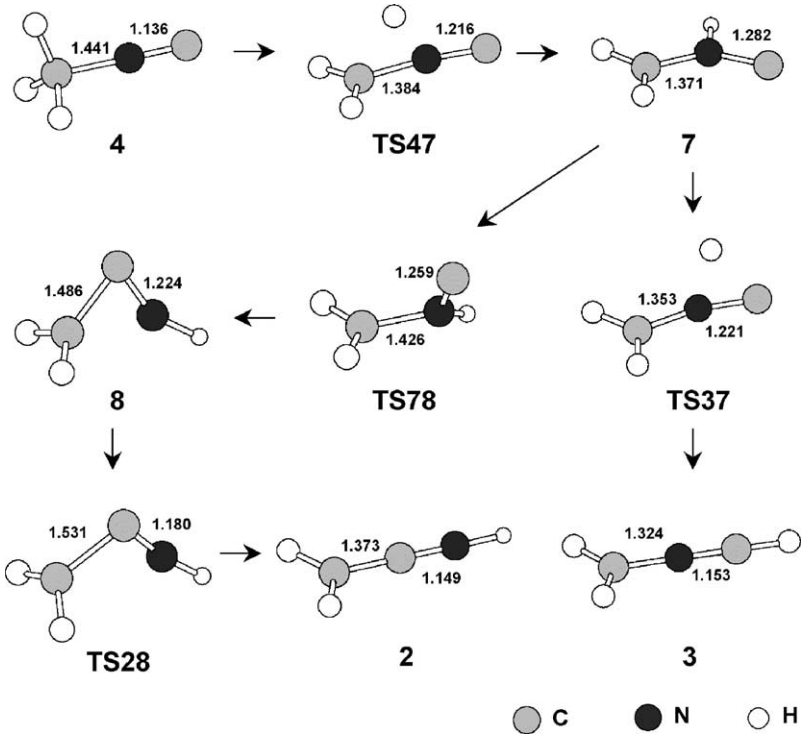

Fig. 3. The isomerization pathway of $CH_3NC^{\bullet+}$ obtained by DFT/UB3LYP/6-311++G(3df,3pd) calculations. The numbers are the bond lengths in Å.

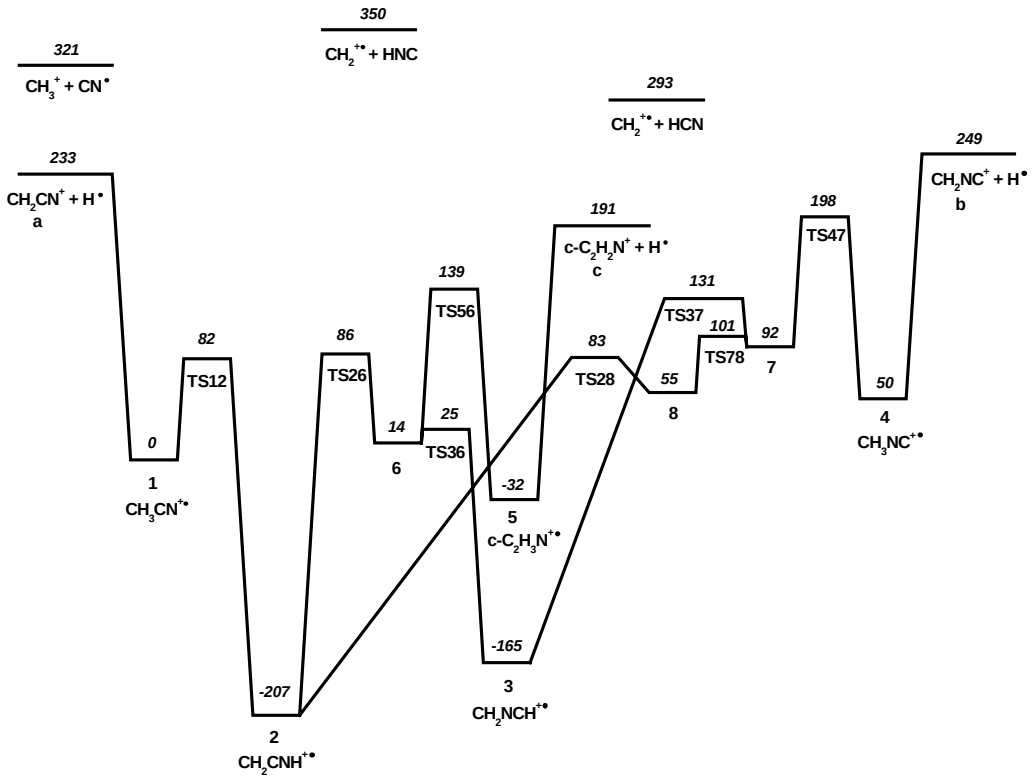

Fig. 4. The potential energy surface calculated at the UB3LYP/6-311++G(3df,3pd) DFT level. The italic numbers are the potential energies in kJ mol^{-1} at the zero point referred to that of **1**.

2 and **3** can undergo further isomerizations to **4**. Fig. 3 shows the isomerization pathway starting from **4**. **4** maintains C_{3V} molecular symmetry upon ionization unlike **1**. By a 1,2-H shift, **4** forms an intermediate (**7**) having planar structure that further isomerizes to **2** by a CNC skeletal rearrangement via **8**. **2** can further isomerize to **3** as described above. Alternatively, **7** can isomerize directly to **3** by a 1,2-H shift.

The PES in Fig. 4 shows that it is energetically favorable for **1** to isomerize to **2** and **3**, but not to **4**. On the other hand, starting from **4**, most of the stable isomers found here can be energetically accessible. Since van Thuijl et al. [4] suggested $CHCHNH^{\bullet+}$ as another stable isomer in their CID study, its geometry was optimized also. However, it is too unstable comparing to **1** (relative energy = 162 kJ mol^{-1}) and can be ruled out as an important intermediate in the dissociation of **1**.

4.2. The H loss

According to the obtained PES, **1** can produce either **a** or **c** by H loss while the production of **b** is less probable. Obviously below the dissociation limit (233 kJ mol^{-1}) to **a**, **1** or its more stable isomers dissociate exclusively to **c** because all the isomerization barriers (**TS12**, **TS26**, **TS56**) lie below the final dissociation step, $\mathbf{5} \rightarrow \mathbf{c} + H^{\bullet}$. RRKM rate calculations were performed based on the obtained PES using the formalism in Eq. (1). The RRKM rate constant calculated with $\Delta S^{\ddagger}$ of 29 J mol^{-1} K^{-1} for the dissociation $\mathbf{1} \rightarrow \mathbf{a}+H^{\bullet}$ is 7.2×10^6 s^{-1} at 0.01 eV above the threshold. Those for the forward ($\mathbf{1} \rightarrow \mathbf{2}$) and reverse ($\mathbf{2} \rightarrow \mathbf{1}$) isomerizations are 3.6×10^{12} and 6.6×10^9 s^{-1}, respectively at the same energy. The σ values of 3 and 1 were used in the calculations, respectively. This indicates that most acetonitrile cations undergo the isomerization to **2** near the dissociation threshold. This result agrees with the suggestions by the PI [7] and SID [8] studies as mentioned in Section 1. Some of **2** can isomerize further to **3**. The further isomerization to **4** is less probable since the final barrier (**TS47**) along the pathway is higher than the dissociation limit to **c**. Namely, **1**, **2**, and **3** can interconvert near or below the dissociation threshold with the largest abundance of **2**. However, at high internal energy the direct H loss from **1** can be more favorable than its isomerization to **2** because the former is a simple bond cleavage, which is entropically more favorable while the latter is a rearrangement reaction. According to the RRKM calculation, the crossover between the two rate-energy curves for the above competitive reactions occurs at 5.2 eV of internal energy of **1**. Namely, the direct H loss can occur dominantly without isomerization to **2** far above internal energy of 5.2 eV. The production of **a** can occur also after the equilibration of **1**, **2**, and **3**, which will be described below.

Estimation of the observed rate constant for the production of **a** or **c** is not simple because several wells are present along the pathway to the products. To simplify the calculation, the PES is approximated to have only double wells. It is assumed that all the acetonitrile cations isomerize to **2** initially and **TS56** is taken as only one transition state between **2** and **5** since the final step through it ($\mathbf{6} \rightarrow \mathbf{5}$) is the rate-determining step in the formation of **5**. As a confirmation of the former assumption, we carried out the MID experiment for $C_2H_3N^{\bullet+}$ from butyronitrile, known to have the structure of **2** [4,5]. The MID profile of the H loss was essentially the same with that in Fig. 1(a) within experimental error limits, indicating free interconversion of **1** and **2** prior to MID. In addition, the dissociation channel to **b** through **4** is ignored, even though it may be important at internal energy far above the dissociation threshold. Then, the kinetic scheme for the H loss can be written simply as follows.

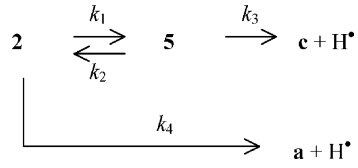

(3)

The expressions for the rates of production of **c** and **a** can be written as below if **5** is not present initially [20,31].

$$\frac{d[\mathbf{c}]}{dt} = \frac{k_1 k_3}{\lambda_+ - \lambda_-}(e^{-\lambda_- t} - e^{-\lambda_+ t}) \tag{4}$$

$$\frac{d[\mathbf{a}]}{dt} = \frac{k_4}{\lambda_+ - \lambda_-}[(\lambda_+ - k_1 - k_4)e^{-\lambda_- t} - (\lambda_- - k_1 - k_4)e^{-\lambda_+ t}] \tag{5}$$

where

$$\lambda_\pm = \tfrac{1}{2}[k_1 + k_2 + k_3 + k_4 \pm \sqrt{(k_2 + k_3 - k_1 - k_4)^2 + 4k_1k_2}] \tag{6}$$

The individual rate constants were calculated using the RRKM formalism. The σ values used are 1, 2, 1, and 1 in the calculations of $k_1 - k_4$, respectively. The rapid interconversions of **2** to the other stable isomers prior to dissociation were considered in the calculations of k_1 and k_4. Only the interconversion to **3** was important, and hence, the sum of densities of states of **2** and **3** was used for ρ in Eq. (1) [20]. The calculated individual rate constants are shown in Fig. 5 as a function of the ion internal energy together with λ_+ and λ_-. Since λ_+ is larger than λ_-, k_1, and k_4 by more than two orders of magnitude in the whole energy range calculated, Eqs. (4) and (5) are simplified to get the abundance ratio of the product ions.

$$\frac{[\mathbf{c}]}{[\mathbf{a}]} \approx \frac{k_1 k_3}{k_4 \lambda_+} \tag{7}$$

The abundance ratio [**c**]/[**a**] calculated is shown as a function of the ion internal energy in Fig. 5(b). This calculation shows that the observed dissociation rate for the H loss is determined by λ_-, and **c** is produced predominantly from the threshold to **c** up to ~1 eV above. The calculated λ_- curve

predicts that the dissociation slightly above the threshold to **c** (0.1–0.3 eV) occurs on the time scale corresponding to the MID in rate constants 10^4 to $10^6\ s^{-1}$. This result shows that the RRKM model calculation based on the simplified PES can explain properly both the detection of the MID and the structure of the product ion, **c**. However, it is to be noted that the production of **a** is more favorable at internal energy of **1** higher than ~3 eV according to the present model calculation.

Uncertainty is remained in the above calculations since we assumed the looseness of the TSs in the calculations of k_3 and k_4 by using $\Delta S^{\ddagger}$ as a typical value 29 J mol^{-1} K^{-1}. To estimate the uncertainty arising from the unknown looseness, the same calculations were carried out using the $\Delta S^{\ddagger}$ value of 46 or 13 J mol^{-1} K^{-1} representing an extremely or barely loose TS, respectively. The main picture described above is not altered. The resultant rate constants (k_3, k_4, λ_+, and λ_-) and [**c**]/[**a**] ratio are somewhat larger or smaller than those obtained above. The uncertainty estimated thus is shown in Fig. 5 as the vertical bar.

The MID of **3** and **4**, reported in the previous studies [4,5], can be explained also. According to the PES obtained above, **3** can produce **c** via **2** and **5**. Since the barrier for the isomerization **4** → **7** is below the direct dissociation (**4** → ***b*** + H$^{\bullet}$) limit, most of **4** near the dissociation limit undergo isomerization to more stable ions, **2** and **3** followed by dissociation to **c**. As increasing internal energy, however, the competition of the direct dissociation channel becomes more important. Since **3** and **4** dissociate to **c** via the most stable isomer **2**, their observed dissociation rates near the threshold will be similar with that obtained above.

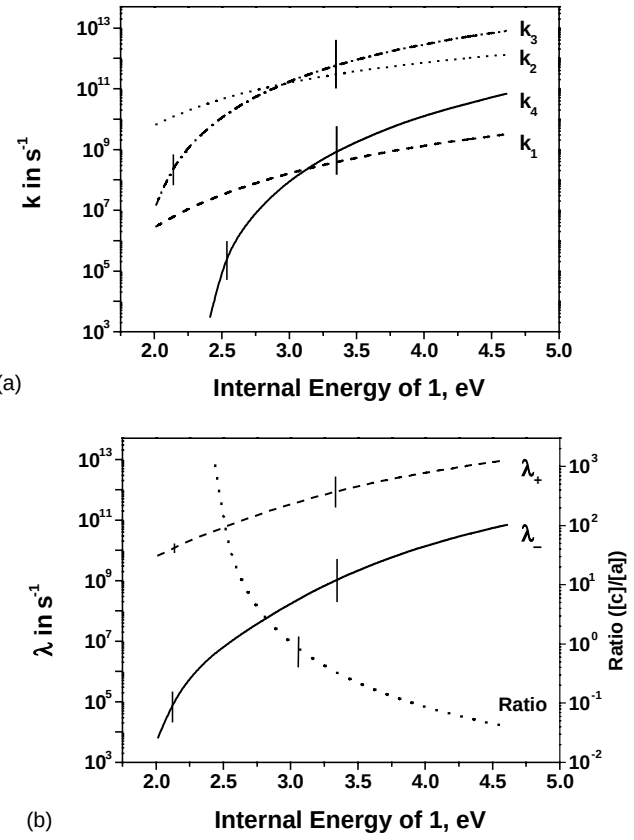

Fig. 5. (a) RRKM rate-energy dependences for $k_1 - k_4$. (b) Energy dependences of λ_+, λ_-, and the abundance ratio [**c**]/[**a**] calculated using Eqs. (6) and (7). The vertical bar in the curves of k_3, k_4, λ_+, λ_-, and [**c**]/[**a**] ratio denotes the uncertainty arising from the unknown looseness of TSs in the calculations of k_3 and k_4. See text for details.

The prediction that the MIDs of **1**–**4** produce a common $C_2H_2N^+$, **c**, agrees with the CID result characterizing the $C_2H_2N^+$ ions produced by MID from **1**–**4** by Chess et al. [5] From the measurement of the appearance energies for the production of $C_2H_2N^+$ from CH_3CN and CH_3NC by Holmes and Mayer [6], the enthalpies of formation at 298 K of the product ion were estimated, 1200 and 1190 kJ mol^{-1}, respectively. The investigators measured also the KERs ($T_{0.5}$, measured at half-height) for the H losses from $CH_3CN^{\bullet+}$ and $CH_3NC^{\bullet+}$, which were 141 and 150 meV, respectively. These similar energetic data mean that the two precursor ions produce a common $C_2H_2N^+$ ion by H loss via a common $C_2H_3N^{\bullet+}$ intermediate, which can be assigned as **c** and **5**, respectively, from the present result. However, the enthalpy of formation (1140 kJ mol^{-1}) of $C_2H_2N^+$ estimated from the experiment for 1*H*-1,2,3-triazole, was smaller than the above ones even though the corresponding $T_{0.5}$ (146 meV) was similar. This indicates that the latter $C_2H_2N^+$ ion may be produced via another intermediate, or its structure may be different from **c**. Since it is unclear which $C_2H_3N^{\bullet+}$ isomer is formed from the triazole cation by N_2 loss, the details on the dissociation will not be further discussed.

A final exit channel in a dissociation pathway can be effectively understood by investigation of the KER. The method to evaluate KERD from a MIKE profile is well established [32]. The KERD for the H loss obtained by analyzing the profile in Fig. 1(a) is shown in Fig. 1(b). The maximum KER is around 0.3 eV which can be accepted as the available energy ($E - E_0$) of the $C_2H_3N^{\bullet+}$ ions undergoing the MID. At this energy, the corresponding rate constant estimated from the obtained λ_- curve is $1 \times 10^6\ s^{-1}$. Even though this value is in the range of typical MID, 10^4 to $10^6\ s^{-1}$, it is larger than the rate constant ($1.2 \times 10^5\ s^{-1}$) estimated in this work. However, the disagreement is not so large considering the several approximations made for the expectation of the rate-energy curve (λ_-) and the limit of the calculated molecular parameters. This indicates that the actual dissociation rate would rise slower with internal energy than expected from the λ_- curve.

Accepting that **5** → **c** + H$^{\bullet}$ is the final step in the H loss, the KERD would be sharp with high probability near the zero KER, which is typical in simple bond cleavages. However, the experimental KERD in Fig. 1(b) shows very broad shape with no probability near the zero KER. The average KER calculated from the distribution is 146 meV. Since it is known that PST can explain properly KERDs for dissociation without a considerable reverse barrier such as

simple bond cleavages, the PST calculation was performed for the production of **c** using the formalism of Eq. (2). The molecular parameters used in the calculation are listed in Table 1. Satisfactory agreement between the experimental and theoretical KERDs could not be obtained using any internal energy of the $C_2H_3N^{\bullet+}$ ions. The theoretical KERD calculated using the available energy 0.3 eV estimated from the experimental maximum KER is shown in Fig. 1(b). The structure in the distribution is due to a quantum effect mainly arising from available limited vibrational quanta of the product ion. The average KER is 96 meV. The experimental KERD is broader than and different in shape from the statistically calculated one.

One possibility for this large experimental KER is that there is a considerable reverse barrier in the final step in the MID, which was suggested in the study by Holmes and Mayer [6]. Then, the KER would be larger than statistically expected. In some direct bond cleavage reactions to produce cations with aromatic stability, reverse barriers have been found experimentally and theoretically [33–38]. Especially in the production of cyclopropenium cation from cyclopropene cation, which is isoelectronic to the dissociation **5** → **c** + $H^{\bullet}$, presence of a reverse barrier was reported [33]. We attempted but failed to locate a transition state between **5** and **c** + $H^{\bullet}$ by quantum chemical calculation, however. The distance between the adjacent N and H atoms of **5** was increased with optimization of all other coordinates at the UB3LYP level using the 6-311++G(3df,3pd) or aug-cc-pVTZ basis set. No reverse barrier was found in the dissociation pathway up to the N–H distance longer than 3.5 Å. We searched for but did not find any other stable $C_2H_2N^+$ isomer not mentioned above, agreeing with the previous theoretical results [12,13]. The other possibility is that PST is not valid for the H loss from **5** even though it occurs via a loose transition state. It has been reported that KERs for H losses could be much greater than expected from PST by Lifshitz (references therein [39]). The dynamic effect in H loss can be significant more than expectation by PST. It is very rare to report successful expectation for KER for H loss by PST [40]. The latter possibility is more reasonable at the moment. Further theoretical studies are needed to understand the measured large KER.

4.3. The productions of CH_3^+ and $CH_2^{\bullet+}$

The other dissociation channels to produce lower *m*/*z* ions are opened at higher internal energies. The most characteristic feature in the dissociation at high internal energy, observed in the experimental studies by CID [4,5] and EI [1,2], is the productions of *m*/*z* 15 and 14 ions, CH_3^+ and $CH_2^{\bullet+}$, respectively. Their relative abundances from several precursors reported are summarized in Table 3. The original data were adjusted so that the total abundance of CH_3^+ and $CH_2^{\bullet+}$ is normalized to 100. The CID results show that the production of CH_3^+ is more favorable relatively in the precursors containing methyl groups. This may be misinterpreted as that the four $C_2H_3N^{\bullet+}$ isomers do not interconvert prior to dissociation. However, it is to be noted that in a CID process precursor ions having a considerable range of internal energy, generated by either EI or dissociation from other molecular ions, are activated by collision. The CID results can be interpreted with the PES obtained in this work. The relative energies for the production of $CH_3^+ + CN^{\bullet}$, $CH_2^{\bullet+} + HCN$, and $CH_2^{\bullet+} + HNC$ are similar comparing to the precursors (Table 2 and Fig. 4). In the CID of **1** or **4** containing a methyl group, the precursor having internal energy below its first isomerization barrier **TS12** or **TS47**, respectively, would maintain its original structure before collisional activation, while that above the barrier would isomerize to other more stable isomers, **2** and **3**. The collisional activation from the former can lead to the production of CH_3^+ preferentially, while that from the latter the production of $CH_2^{\bullet+}$. Both the processes can contribute significantly to the CID signals, of which abundances are determined by detailed kinetic factors. On the other hand, in the CID of **2** and **3** most of the precursor ions maintain their original structures or interconvert each other before collisional activation, and dissociate to $CH_2^{\bullet+}$ preferentially by collisional activation.

Table 3
Abundance ratios (CH_3^+:$CH_2^{\bullet+}$) reported in the CID and EI studies

Precursors	CID1[a]	CID2[b]	EI
1 ($CH_3CN^{\bullet+}$)	25:75	21:79	18:82[c]
2 ($CH_2CNH^{\bullet+}$)	13:87	12:88	
3 ($CH_2NCH^{\bullet+}$)	5:95		
4 ($CH_3NC^{\bullet+}$)	49:51	55:45	65:35[d]

[a] Ref. [5]: acetonitrile, butyronitrile, *n*-propyl isocyanide, and methyl isocyanide were used for CID of **1**–**4**, respectively.
[b] Ref. [4]: acetonitrile, butyronitrile, and methyl isocyanide were used for CID of **1**, **2**, and **4**, respectively.
[c] Ref. [1]: 70 eV EI of acetonitrile.
[d] Ref. [2]: 70 eV EI of methyl isocyanide.

More abundant production of CH_3^+ in the CID and EI of **4** than in **1** can be interpreted also with the present PES. If other conditions are similar, the barrier heights for the direct production of CH_3^+ and the first isomerization to produce $CH_2^{\bullet+}$ will determine the relative abundance of CH_3^+ and $CH_2^{\bullet+}$. The difference of the barrier heights in **4** is 123 kJ mol^{-1}, which is far smaller than that in **1**, 219 kJ mol^{-1}. This means that the production of CH_3^+ competes more effectively with the first isomerization to produce $CH_2^{\bullet+}$ in the dissociation of **4** than in **1**. This would result in the rich production of CH_3^+ in the dissociation of **4** relative to **1**.

5. Conclusions

The structures and potential energies of various $C_2H_3N^{\bullet+}$ isomers were calculated at the UB3LYP/6-311++G(3df, 3pd) level. By connecting them with the transition states the PES for the H loss reactions was constructed. Three

isomers were found to be more stable than $CH_3CN^{\bullet+}$, which are $CH_2CNH^{\bullet+}$, $CH_2NCH^{\bullet+}$, and c-$C_2H_3N^{\bullet+}$ in order of decreasing stability. The RRKM model calculations based on the PES showed that $CH_3CN^{\bullet+}$ interconverts with $CH_2CNH^{\bullet+}$ and $CH_2NCH^{\bullet+}$ near and below the threshold for the H loss, but does not with $CH_3NC^{\bullet+}$ because of presence of a considerable barrier. From the RRKM rate calculation with the simplified double well PES for the productions of c-$C_2H_2N^+$ and CH_2CN^+, the observation of the MID on a microsecond time scale for the H loss from $CH_3CN^{\bullet+}$ could be understood. The present theoretical calculations predict that the MIDs from the four stable molecular cations, $CH_3CN^{\bullet+}$, $CH_2CNH^{\bullet+}$, $CH_2NCH^{\bullet+}$, and $CH_3NC^{\bullet+}$, occur via an identical intermediate, the cyclic $C_2H_3N^{\bullet+}$ isomer, to produce the cyclic $C_2H_2N^+$ cation. At higher internal energy, CH_2CN^+ or CH_2NC^+ can be produced by H loss. The measured KERD for the MID was large and could not be explained with the statistical phase space theory even though a reverse barrier was not found theoretically in the production of c-$C_2H_2N^+$. The productions of CH_3^+ and $CH_2^{\bullet+}$ from the $C_2H_3N^{\bullet+}$ isomers reported previously could be interpreted with the PES obtained. Further kinetic studies such as dissociation rate measurements for energy-selected molecular cations will aid in constructing a more realistic PES with better accuracy in energetics.

Acknowledgements

The author thanks Prof. Myung Soo Kim for use of the mass spectrometer and Dr. Jeong Hee Moon for helpful discussions on quantum chemical calculations.

References

[1] W. Heerma, J.J. de Ridder, G. Dijkstra, Org. Mass Spectrom. 2 (1969) 1103.
[2] W. Heerma, J.J. de Ridder, Org. Mass Spectrom. 3 (1970) 1439.
[3] P.W. Harland, B.J. McIntosh, Int. J. Mass Spectrom. Ion Processes 67 (1985) 29.
[4] J. van Thuijl, J.J. van Houte, A. Maquestiau, R. Flammang, C. DeMeyer, Org. Mass Spectrom. 12 (1977) 196.
[5] E.K. Chess, R.L. Lapp, M.L. Gross, Org. Mass Spectrom. 17 (1982) 475.
[6] J.L. Holmes, P.M. Mayer, J. Phys. Chem. 99 (1995) 1366.
[7] D.M. Rider, G.W. Ray, E.J. Darland, G.E. Leroi, J. Chem. Phys. 74 (1981) 1652.
[8] C. Mair, J. Roithová, J. Fedor, M. Lezius, Z. Herman, T.D. Märk, Int. J. Mass Spectrom. 223/224 (2003) 279.
[9] E. Marotta, R. Seraglia, F. Fabris, P. Traldi, Int. J. Mass Spectrom. 228 (2003) 841.
[10] E. Marotta, P. Traldi, Rapid Commun. Mass Spectrom. 17 (2003) 2846.
[11] D.J. Swanton, G.B. Bacskay, G.D. Willett, N.S. Hush, J. Mol. Struct. (THEOCHEM) 91 (1983) 313.
[12] P.W. Harland, R.G.A.R. Maclagan, H.F. Schaefer, J. Chem. Soc., Faraday Trans. II 85 (1989) 187.
[13] P.M. Mayer, M.S. Taylor, M.W. Wong, L. Radom, J. Phys. Chem. A 102 (1998) 7074.
[14] C.E. Hudson, D.J. McAdoo, Int. J. Mass Spectrom. 219 (2002) 295.
[15] D.J. McAdoo, Mass Spectrom. Rev. 19 (2000) 38.
[16] R.G. Cooks, J.H. Beynon, R.M. Caprioli, G.R. Lester, Metastable Ions, Elsevier, Amsterdam, 1973.
[17] M.J. Frisch, G.W. Trucks, H.B. Schlegel, G.E. Scuseria, M.A. Robb, J.R. Cheeseman, J.A. Montgomery, Jr., T. Vreven, K.N. Kudin, J.C. Burant, J.M. Millam, S.S. Iyengar, J. Tomasi, V. Barone, B. Mennucci, M. Cossi, G. Scalmani, N. Rega, G.A. Petersson, H. Nakatsuji, M. Hada, M. Ehara, K. Toyota, R. Fukuda, J. Hasegawa, M. Ishida, T. Nakajima, Y. Honda, O. Kitao, H. Nakai, M. Klene, X. Li, J.E. Knox, H.P. Hratchian, J.B. Cross, C. Adamo, J. Jaramillo, R. Gomperts, R.E. Stratmann, O. Yazyev, A.J. Austin, R. Cammi, C. Pomelli, J.W. Ochterski, P.Y. Ayala, K. Morokuma, G.A. Voth, P. Salvador, J.J. Dannenberg, V.G. Zakrzewski, S. Dapprich, A.D. Daniels, M.C. Strain, O. Farkas, D.K. Malick, A.D. Rabuck, K. Raghavachari, J.B. Foresman, J.V. Ortiz, Q. Cui, A.G. Baboul, S. Clifford, J. Cioslowski, B.B. Stefanov, G. Liu, A. Liashenko, P. Piskorz, I. Komaromi, R.L. Martin, D.J. Fox, T. Keith, M.A. Al-Laham, C.Y. Peng, A. Nanayakkara, M. Challacombe, P.M.W. Gill, B. Johnson, W. Chen, M.W. Wong, C. Gonzalez, J.A. Pople, Gaussian 03 (Revision B.04), Gaussian, Inc., Pittsburgh, PA, 2003.
[18] A.P. Scott, L. Radom, J. Phys. Chem. 100 (1996) 16502.
[19] P.J. Robinson, K.A. Holbrook, Unimolecular Reactions, Wiley, New York, 1972.
[20] T. Baer, W.L. Hase, Unimolecular Reaction Dynamics: Theory and Experiments, Oxford, New York, 1996.
[21] C. Lifshitz, Mass Spectrom. Rev. 1 (1982) 309.
[22] C. Lifshitz, Adv. Mass Spectrom. 11 (1989) 713.
[23] J.C. Light, J. Chem. Phys. 40 (1964) 3221.
[24] W.J. Chesnavich, M.T. Bowers, J. Am. Chem. Soc. 98 (1976) 8301.
[25] W.J. Chesnavich, M.T. Bowers, J. Chem. Phys. 66 (1977) 2306.
[26] J.C. Choe, B.J. Kim, M.S. Kim, Bull. Kor. Chem. Soc. 10 (1989) 167.
[27] J.J. Butler, M.L. Fraser-Monteiro, L. Fraser-Monteiro, T. Baer, J.R. Hass, J. Phys. Chem. 86 (1982) 747.
[28] T. Baer, P.M. Mayer, J. Am. Soc. Mass Spectrom. 8 (1997) 103.
[29] D.R. Lide (Ed.), Handbook of Chemistry and Physics, 76th ed., CRC Press, Cleveland, 1995.
[30] S.G. Lias, J.E. Bartmess, J.F. Liebman, J.L. Holmes, R.D. Levine, W.G. Mallard, J. Phys. Chem. Ref. Data 17 (Suppl. 1) (1988).
[31] T. Baer, W.A. Brand, T.L. Bunn, J.J. Butler, Faraday Discuss. Chem. Soc. 75 (1983) 45.
[32] I.C. Yeh, M.S. Kim, Rapid Commun. Mass Spectrom. 6 (115) (1992) 293.
[33] G. Frenking, H. Schwarz, Int. J. Mass Spectrom. Ion Phys. 52 (1983) 131.
[34] C. Lifshitz, Y. Gotkis, A. Ioffe, J. Laskin, S. Shaik, Int. J. Mass Spectrom. Ion Processes 125 (1993) R7.
[35] V. Hrouda, P. Cársky, M. Ingr, Z. Chval, G.N. Sastry, T. Bally, J. Phys. Chem. A 102 (1998) 9297.
[36] W.G. Hwang, J.H. Moon, J.C. Choe, M.S. Kim, J. Phys. Chem. A 102 (1998) 7512.
[37] D.Y. Kim, J.C. Choe, M.S. Kim, J. Phys. Chem. A 103 (1999) 4602.
[38] D.S. Won, J.C. Choe, M.S. Kim, Rapid Commun. Mass Spectrom. 14 (2000) 1110.
[39] C. Lifshitz, Int. J. Mass Spectrom. Ion Phys. 118/119 (1992) 315.
[40] A.J. Illies, M.F. Jarrold, M.T. Bowers, J. Am. Chem. Soc. 104 (1982) 3587.